Enhanced Heat Transfer, 1998, Vol. 5, pp. 39–52
Reprints available directly from the publisher
Photocopying permitted by license only

Heat Transfer and Pressure Drop During Evaporation and Condensation of R22 inside 9.52-mm O.D. Microfin Tubes of Different Geometries

A. MUZZIO, A. NIRO and S. AROSIO

Dipartimento di Energetica, Politecnico di Milano piazza Leonardo da Vinci 32, 20133 Milano, Italy

(Received 6 March 1997; In final form 11 July 1997)

Saturated flow boiling and convective condensation experiments for oil-free Refrigerant-22 have been carried out with a microfin tube with a new cross-section profile, as well as with two traditional microfin tubes and with a smooth one. All tubes have the same outer diameter. Data are for mass fluxes ranging from about 90 to 400 kg/m^2·s. In boiling tests, the nominal saturation temperature is 5 °C, with inlet quality varying from 0.2 to 0.6 and the quality variation along the test section ranging from 0.1 to 0.5. In condensation, results are for saturation temperature equal to 35 °C, with inlet and outlet qualities of 0.8 and 0.2, respectively. The new microfin tube shows the best thermal performances among the microfin tubes tested, especially in evaporation. For this case, the enhancement factor comes up to 4. Experimental results for microfin tubes are compared with predictions of a correlation scheme recently proposed; these predictions correlate well only with data for the microfin tube with a geometry much similar to one accounted by the scheme.

Keywords: Heat transfer, enhanced flow boiling, convective condensation, microfin tubes

1. INTRODUCTION

In heat exchangers for air-conditioners and refrigerators, the reduction of the air-side thermal resistance to a value comparable to that of the refrigerant-side has induced industry to improve the thermal performance of this side. As discussed by Bergles [1994] and Thome [1990], several techniques may be employed for heat transfer enhancement of in-tube evaporation and condensation, even if any of them increases the pressure drop. Currently, microfin tubes, i.e., tubes with numerous, very small integral fins on the inner surface, are widely used (nowadays, more than 30% of the tubing in refrigerating and air-conditioning are micro finned) because they can substantially enhance heat transfer coefficients with a small pressure drop penalty. Thus, in recent years, many efforts have been spent in designing and developing microfin geometries which could provide high heat transfer coefficients and low pressure drop increment.

Reliable prediction of boiling and condensation heat transfer coefficients inside microfin tubes is a

key-factor for their successful use. Advances have been made in predictive methods as discussed by Webb [1994] or reviewed by Darabi *et al.* [1995]. However, a really trustworthy evaluation of heat transfer coefficients remains experimental because of complex fluid-dynamic and heat transfer processes involved in flow boiling and convective condensation in these tubes. For the same reason, the development of more efficient microfin geometries is essentially an empirical art still.

Heat transfer characteristics of microfin tubes have been extensively studied over the past 18 years. Schlager *et al.* [1990], Thome [1994] and Kandlikar and Raykoff [1996] list about 30 papers that report on experimental results in evaporation and condensation inside microfin tubes with halocarbons refrigerants. In spite of the amount of published results, there is still a large demand of further experimental research in order both to test new microfin geometries and to gain a deeper understanding of boiling and condensation mechanisms in these tubes. The latter is an essential condition for the development of general correlations which can accurately predict heat transfer and friction characteristics on such surfaces over a wide range of geometries.

Moved by these reasons, we are currently performing an experimental investigation on flow boiling and convective condensation of halocarbon refrigerants inside microfin tubes as reported by Arosio *et al.* [1995, 1996]. This paper reports on average heat transfer coefficients and pressure drops during evaporation and condensation of oil-free R-22 inside a microfin tube with a new cross-section profile, compared with those of two traditional microfin tubes. Data for a smooth tube, referred to as the reference case, are also reported. All tubes have the same outer diameter and are horizontally operated.

Experimental results for the smooth tube are compared with the estimates obtained by several available correlations. The correlations proposed by Chawla [1967], Kandlikar [1990], Liu-Winterton [1991], and Pierre [1964] are considered for the boiling coefficient, whereas data on heat transfer during condensation are correlated using the correlations of Shah [1979] and Cavallini-Zecchin [1972], and the calculation schemes proposed by Butterworth [1983] and by Paikert [1988]. In addition, the pressure drop data are correlated using the correlations proposed by Chawla, Grønnerud [1972], Friedel [1979] (only for boiling data) and Rohsenow [1985] (only for condensation data).

Finally, we also present comparison between values of boiling coefficients measured in microfin tubes, and predictions obtained with the correlation scheme recently proposed by Kandlikar and Raykoff [1996]. Since this correlation contains some empirical constants which depend on specific geometry, its predictions correlate well only with data for the microfin tube whose section is similar to one accounted by the scheme.

2. EXPERIMENTAL APPARATUS

The schematic diagram of the experimental facility is shown in Figure 1. The rig consists of three circuits, namely, a sealed refrigerant (R-22) circuit, a water circuit to heat or cool the refrigerant in the test section, and a chilled coolant (water-glycol solution) circuit.

The main components of the refrigerant circuit are a boiler, the test section, a condenser, a gear pump and a filter dryer. The boiler is a 58 dm^3, stainless-steel pressure vessel of cylindrical shape with welded ellipsoidal heads; a heater, consisting of three electrical cartridges of 1, 1.5 and 2.5 kW power, is placed in the boiler bottom. Liquid and vapor are drawn from the boiler through two distinct lines. On each line two float-type flowmeters, whose float is magnetically coupled to the indicating scale, are installed to measure the volume flow rates of refrigerant stream. A double-pipe subcooler is mounted on the liquid line upstream of the flowmeters to ensure a single phase flow through them for any operating conditions. For the same reason, a ribbon electrical heater is wounded around the vapor line

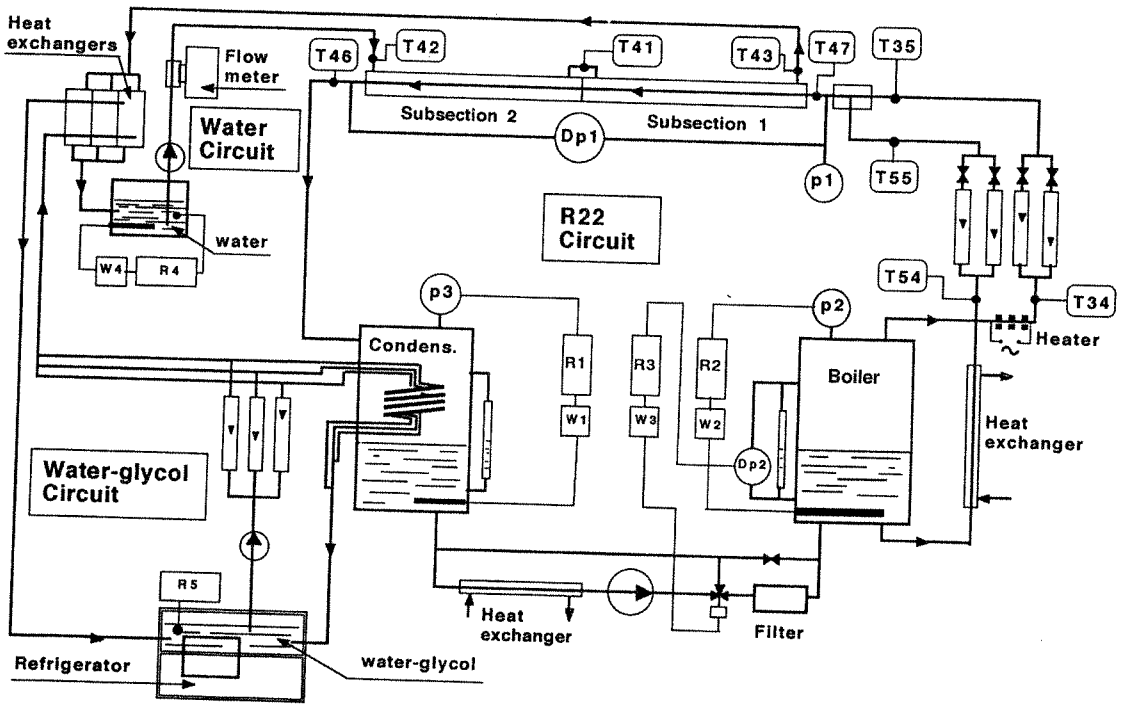

FIGURE 1 Schematic diagram of experimental apparatus.

upstream of the flowmeters. The liquid and vapor flow rates are controlled by precision metering valves. Downstream of the valves, vapor is mixed with liquid; the two-phase mixture flows through a 1.5 m long calming section and then enters the test section. At the exit, refrigerant flows through a second calming section (1.8 m) and then is discharged to the condenser, which maintains the test section outlet pressure at a given value. The condenser is a pressure vessel with the same shape and dimension as the boiler; three round coil heat exchangers are located inside the upper part of condenser; an electrical cartridge of 1 kW power is mounted in the condenser bottom. Finally, the liquid phase of the refrigerant is drawn from the condenser by a gear pump and is conveyed through a filter dryer to the boiler. Another double-pipe heat exchanger is mounted on the pump suction line to ensure a liquid flow through the pump. Refrigerant temperature is measured upstream of the flowmeters, downstream of the controlling valves, and at the inlet and outlet of the test section by thermocouples inserted in 60 mm long, 3 mm o.d., stainless steel L-shaped wells located on the duct axis.

The test section is a straight, 2.6 m long, 9.52 mm o.d., copper tube that is divided in two identical parts, which we refer to as subsections. They are connected to each other and to the loop, without any change in the duct internal diameter, via three 3-way 12-mm tee fittings. Two pressure-taps are drilled in each junction; the gap between the inner surface of the fitting and the outer surface of the tube serves as a pressure annular-chamber; pressure taps are connected via a manifold to pressure transducers. The refrigerant pressure is measured with a strain-gauge transducer (2 MPa full scale value), whereas pressure drop along the test section with an inductive differential pressure transducer (25 kPa full scale value, 1% o.f.s. accuracy). Both subsections are equipped with four T-type thermocouples to measure wall

temperatures, which are placed in pairs at 140 mm from either ends; in each pair, the thermocouples are 180 degrees apart. The thermocouple wires are 0.15 mm diameter, and they are cemented in longitudinal grooves (80 mm long, 0.5 mm large and 0.2 mm deep) cut in the outside wall of the tube.

Every subsection is enclosed by a 14 mm i.d. brass tube in order to create an annulus through which the heating or cooling water is circulated. Such a jacket is mounted on the subsection via two tee fittings which also allow the water to enter and leave the annulus. The distance between the inlet and discharge ducts of the jacket is 1.12 m and it is assumed as the active heat transfer length for the subsection. Calming and test sections are insulated by a 10 cm thick, glass-wool annulus, whereas a 2 cm thick, foam plastic sheets or annuli are used for the other circuit components and pipes.

The water circuit consists of a tank provided with a heater, a centrifugal pump, the jackets surrounding the test section, a water-to-water heat exchanger. Demineralized water is drawn from a 30 dm^3, stainless steel tank equipped with a 5 kW-power heater. Water flows inside the jackets surrounding the test section in counterflow with the refrigerant. Downstream the last jacket, water enters a plate heat exchanger in counter flow with the chilled coolant, and then it is discharged into the tank. The volume flow rate of water is measured by an inductive flowmeter (0.15 dm^3/s full scale value). The bulk temperature of the water stream is measured by three thermal probes, located at the inlet of each subsection and at the outlet of the last one, respectively. Each probe consists of three T-type thermocouples cemented in three fine wells drilled in a copper cylinder with an outer diameter of 13 mm and an height of 20 mm. Such a cylinder reduces the area of stream cross-section, thus promoting flow mixing and hence equalisation of the liquid temperature. Furthermore, since thermocouples are connected in series, the measured voltage is proportional to the sum of temperatures taken in three different points of the cylinder; we assumed the temperature corresponding to this voltage as representative of the cylinder mean temperature. A 100 Ω Pt-resistor is employed to measure the water temperature in the tank.

Finally, the chilled coolant circuit is filled with a water-glycol solution and it consists of a commercial refrigeration unit and a centrifugal pump. Such a circuit provides the cold medium circulated in the heat exchangers placed in the refrigerant condenser or mounted on both the refrigerant and the water circuits.

3. TEST PROCEDURES AND DATA REDUCTION

Thermocouple voltages and signals from the pressure transducers and inductive flowmeter are cyclically read by a data acquisition unit HP3497, and sent to an on-line PC. In order to ensure that all measured values are affected by similar RMS relative errors, measurements of the refrigerant temperature and pressure at the test section inlet, as well as of the pressure drop and the water flow rate are based on 30, 50, 50 and 100 readings for cycle, respectively. Furthermore, every experimental data is obtained by averaging measurements from 10 cycles to reduce the influence of random errors and fluctuations.

Temperatures are converted from thermocouples voltages by means of experimental calibration curves specifically and preliminary obtained. Also, calibration curves of the water and refrigerant flowmeters were preliminary checked through mass and thermal power measurements. As a result of such checks, we estimate that volume flow rates of the refrigerant and water are measured with relative errors smaller than 2% and 1% of the reading, respectively, which agree with instrument nominal accuracy. Furthermore, a numerical simulation indicated that a negligible error is made in assuming the inside wall temperature equal to the wall temperature effectively measured. The agreement between wall temperatures, refrigerant inlet and outlet temperatures and the

saturation temperature corresponding to the test section pressure, was checked upon setting a refrigerant two-phase mixture, shut off inside the test section, in thermal equilibrium with a water stream flowing at environmental temperature. As a consequence, the zero off-set of the absolute pressure transducer was slightly adjusted. Finally, thermal resistance of the test section insulation was measured, finding a value of about 4 K/W.

The system start-up consists of the following main procedures. At first, the refrigeration unit is started. As water-glycol solution is cooled, the condenser and boiler pressures are set to values about 0.2 MPa smaller and higher than the test nominal pressure, respectively. At the same time, water temperature is set to a value 2–4 K higher or smaller than the test nominal temperature, depending on whether the test is performed in evaporation or condensation. As soon as the aforementioned values are attained, the mass flow rates of liquid and vapor of R-22 through the test section, as well as of water through the jackets are imposed. For the latter, we choose a value which allows a water temperature drop along the test section no smaller than 2 K. Finally, through many fine adjustments the steady-state condition is achieved at fixed values of temperature, inlet quality and quality change. Because accurate and reproducible data are obtained only if steady-state conditions have been really attained, we assumed on empirical basis to operate steadily when fluctuations of heat flow rate is less than one per cent. Steady-state conditions usually requires about 2.5 hours to be established after system start-up; however, this time reduces to 1.5 hours if system is already "warm".

As the system operates steadily, measurement cycles start. For every operating condition, we collect at least ten experimental data (each resulting by averaging measurements from 10 cycles, as above mentioned) with a test run time of about 60 minutes. If steady-state condition fails during a data collection, the measurement cycle is interrupted and the results logged in that cycle are discarded. At the end of every cycle, the collected experimental data are processed and quantities as mass flow rate, mass flux, inlet quality, heat flow rate and heat transfer coefficients are computed as follows.

The refrigerant mass flow rate is determined from a mass balance over the mixer using the volumetric flow rates of the liquid and the vapor phases, and the corresponding densities evaluated upstream the flowmeters. The mass flux inside the test section is based on a nominal cross-section area with respect to the maximum internal diameter, i.e., the diameter at the root of microfins. The thermodynamic quality at the entrance of the test section is calculated, instead, from an energy balance over the mixer assuming the quality variation along the calming section is negligible. The heat transfer in every subsection is derived from an energy balance on the water flowing through the annulus. Finally, regarding to heat transfer coefficient evaluation, we assume that the refrigerant temperature varies linearly between the value T_{in}, measured at the entrance of the test section, and the value T_{out} computed at the exit as $\tilde{T}_s(\tilde{p}_s(T_{\text{in}}) - \Delta p)$, where $\tilde{T}_s$ is the function that correlates the saturation temperature to the pressure, $\tilde{p}_s$ the inverse function of $\tilde{T}_s$, and Δp the pressure drop measured along the test section. Then, for both subsections we compute the average refrigerant temperature $T_{r.m,i} = 0.5\,(T_{r.\text{in},i} + T_{r.\text{out},i})$ with $i = 1$ or 2, the average wall temperature $T_{w.m,i}$, the temperature mean difference $\Delta T_{m,i} = (T_{w.m,i} - T_{r.m,i})$, and the heat transfer coefficient $h_i = q_i/\Delta T_{m,i}$ where q_i is the average heat flux based on a nominal inside area of the tube. For the latter, we adopted the inside area of the smooth tube. Average heat flux and heat transfer coefficient of the test section are eventually obtained by averaging q_i and h_i, respectively.

Experimental uncertainties for the present investigation are summarised as follows. Pressure drop measurements are affected by an uncertainty equal to the accuracy of the differential transducer (1% at full scale), whereas the relative uncertainty of the other relevant variables-estimated by a propagation error analysis- are: ±2.8% for the

refrigerant mass flow rate, ±1.3% for the inlet quality, ±1.4% for the heat rate, and ±7% for the average heat transfer coefficient.

4. RESULTS AND DISCUSSION

The first test runs were performed on a smooth tube entirely in the subcooled region. These tests provided a check on the experimental procedure reliability and on data validity. The values of heat transfer coefficient in single-phase forced convection collected in these tests are within 5 per cent of the values evaluated by Gnielinski [1983] correlation using the entrance correction-factor derived by Hausen. Furthermore, in these test runs energy balances on the water side and the refrigerant side agreed within 2 per cent.

In saturated flow boiling or convective condensation, for a fixed test section configuration, i.e., dimension and shape of the cross section, length, orientation with respect to gravity, both pressure drop and average heat transfer coefficient depend on four independent variables, namely, total mass flow rate, temperature (or pressure), inlet thermodynamic quality and heat rate. Since quality change along the test section depends linearly on heat rate, a different but equivalent parameterization can be obtained by substituting the former with the latter quantity in the list of independent variables.

The experimental data reported here were obtained on a smooth tube and three microfin tubes with an outer diameter of 9.52 mm. The microfin tubes tested are the Metofin® tubes type 952-30VA40/54A, 930V50 and 928W90, manufactured by Trefimetaux, which we will denote as tubes VA, V and W, respectively. A drawing of their cross-section profiles is reported in Figure 2, whereas values of their geometric parameters are listed in Table I together with dimensions of the smooth tube. This table also lists the total heat transfer internal surface ratio and the actual cross-section ratio with respect to the smooth tube. Tubes W and V are very similar to Hitachi Thermofin™ and Thermofin-EX™, respectively, whereas tube VA is a new microfin tube, developed by Trefimetaux, which is characterised by a reduced number of fins with a sharp shape and two different heights, as shown in Figure 2a. This latter characteristic is the distinguishing feature of tube VA, while the apex and helix angles are features shared with other microfin tubes of new

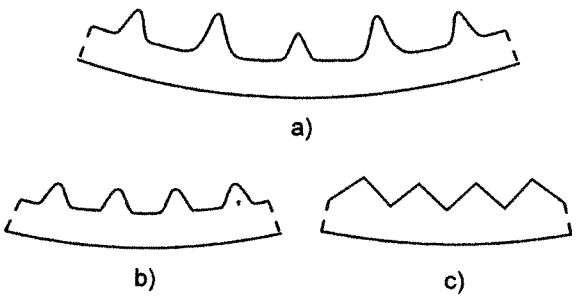

FIGURE 2 Drawing of the cross-sectional profiles of the microfin tubes tested: (a) tube VA, (b) tube V, and (c) tube W.

TABLE I Geometrical parameters of the tested tubes

Parameter	Tube	VA	V	W	Smooth
Outside diameter	[mm]	9.52	9.52	9.52	9.52
Maximum inside diameter	[mm]	8.92	8.92	8.84	8.92
Bottom wall thickness	[mm]	0.30	0.30	0.34	0.30
Higher fin height	[mm]	0.23	0.20	0.15	–
Lower fin height	[mm]	0.16	–	–	–
Apex angle		40°	53°	90°	–
Number of grooves		54	60	65	–
Helix angle		18°	18°	25°	–
Total heat transfer internal suface ratio		1.51	1.51	1.28	1
Actual cross surface ratio		0.963	0.949	0.945	1

design as, for example, the Hitachi Thermofin-HEX™.

Evaporation tests were carried out at a nominal saturation temperature of 5°C(±0.2 K) corresponding to a pressure of 0.58 MPa while, in condensation, the nominal temperature was 35 °C (±0.2 K) corresponding to a pressure of 1.35 MPa. Having fixed the test temperature, three independent variables survive, namely, the total mass flow rate, the inlet thermodynamic quality and the quality change. In order to demonstrate clearly the variation effect of each variable against the others, they were varied in turn while keeping the others constant. In evaporation tests, the total mass flow rate ranged from 5.556 to 25 g/s corresponding to a mass flux G between about 90 and 400 kg/s·m^2, the inlet quality x_{in} was varied from 0.2 to 0.6, and the quality change Δx from 0.1 to 0.5. For $\Delta x = 0.3$, the average heat flux ranges from about 5200 to 24000 W/m^2, being the vaporisation enthalpy equal to 200.3 kJ/kg. In condensation, only the mass flow rate effect was investigated. Total mass flow rate was varied in the same range as in evaporation tests, with the inlet and the outlet nominal qualities equal to 0.8 and 0.2, respectively. In this case, average heat flux ranges from about 9100 to 41000 W/m^2, being the condensation enthalpy equal to 171.6 kJ/kg.

Figure 3 shows the boiling heat transfer coefficient h_b plotted versus the mass flux G for the tested microfin tubes; data obtained on the smooth tube are also included for comparison. For such data, nominal inlet quality and quality change are $x_{in} = 0.3$ and $\Delta x = 0.3$, respectively. As expected, the boiling coefficient is an increasing function of G, and its values for microfin tubes result much higher than those for the smooth tube, although they are characterised by a lower growth rate. The tube VA appears to have the best performance, as it can be also seen in Figure 4 where the evaporation enhancement factor- defined as the ratio of the microfin tube heat transfer coefficient to that of the smooth tube- is plotted versus G. As shown, the tube VA displays an enhancement factor which ranges between about 4

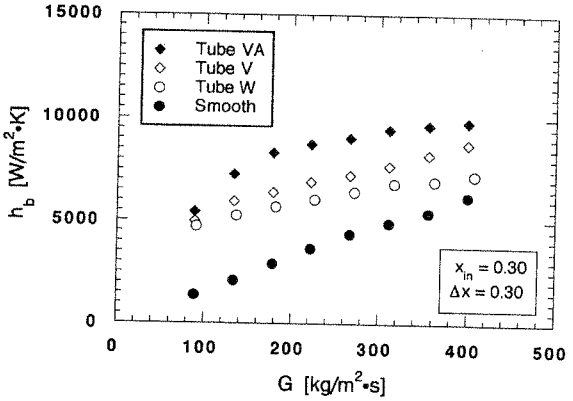

FIGURE 3 Evaporation heat transfer coefficient versus mass flux for given inlet quality and quality change along test section.

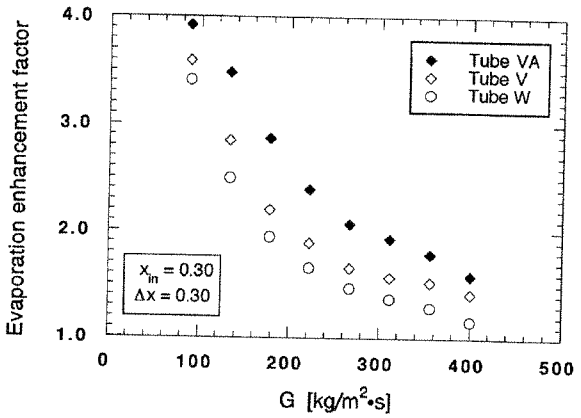

FIGURE 4 Evaporation enhancement factor versus mass flux for given inlet quality and quality change along test section.

and 1.6, with an average increment of 20% with respect to the tube V. The average deviation between enhancement factors for tubes V and W instead is lower, being almost 12% at least for G up to about 310 kg/s·m^2. It is also apparent that the enhancement factor is a decreasing function of G, in agreement with expectation that it should approach the surface ratio at high mass flux.

The effect of the average quality x_m on the evaporation heat transfer coefficient, for fixed mass flux and quality change ($G = 224$ kg/s·m^2, $\Delta x = 0.3$), can be seen on the plot of Figure 5. For the smooth tube, a slightly marked maximum is

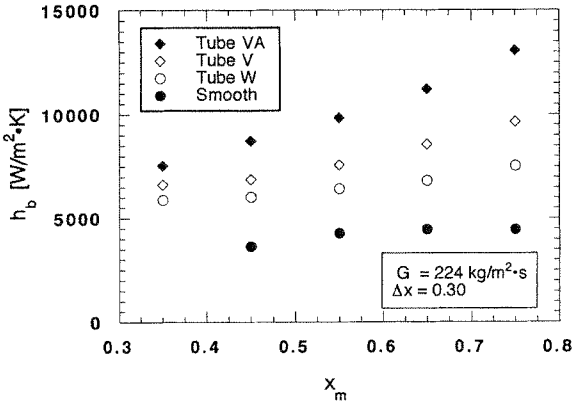

FIGURE 5 Evaporation heat transfer coefficient versus average quality for given mass flux and quality change along test section.

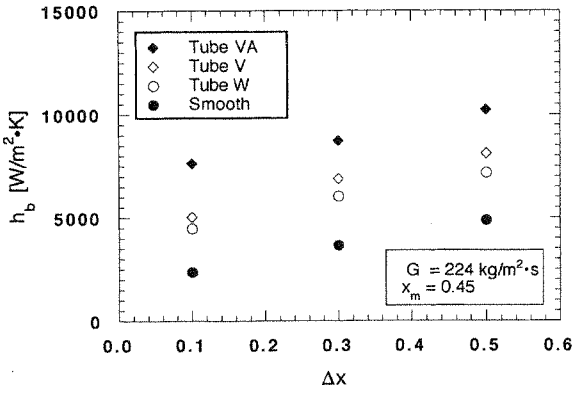

FIGURE 6 Evaporation heat transfer coefficient versus quality change along test section for given mass flux and average quality.

observed, approximately located at $x_m = 0.7$. With local heat transfer coefficients inside a smooth tube, the occurrence of a maximum -more or less pronounced, depending on mass flux- is well established, in the relevant literature, at vapor quality ranging between 0.8 and 0.9. After the maximum, heat transfer coefficient displays a sharp decrement which is attributable to the dryout onset. In the case of average heat transfer coefficients, the averaging process over a quality interval causes a curve flattening and a displacement of the maximum toward lower quality values. For the microfin tubes tested, instead, a continuously increasing trend of the average heat transfer coefficient can be noticed. Hence, it can be inferred that micro finning seems to provide, in addition to the substantial heat transfer enhancement, a shift of the dryout occurrence in the region of higher qualities. Both these effects are markedly exhibited by data for the tube VA.

Regarding the influence of quality change for fixed mass flux and average quality ($G = 224$ kg/s·m^2 and $x_m = 0.45$), data plotted in Figure 6 show that the heat transfer coefficient is also an increasing function of Δx for all tubes with approximately the same growth rate. Values for the tube VA result about 30% higher than those for the tube V; whereas the deviation between this latter and the tube W remains smaller (near 13%) also in this case.

Condensation heat transfer results versus mass flow rate, for fixed inlet and outlet vapor qualities ($x_{in} = 0.8$ and $x_{out} = 0.2$), are shown in Figure 7; for the investigated range of G, the all liquid Reynolds' number varies from about 3500 to 16000. As in evaporation, a substantial heat transfer improvement is achieved by microfin tubes with respect to the smooth tube; however, the heat transfer coefficient is an increasing

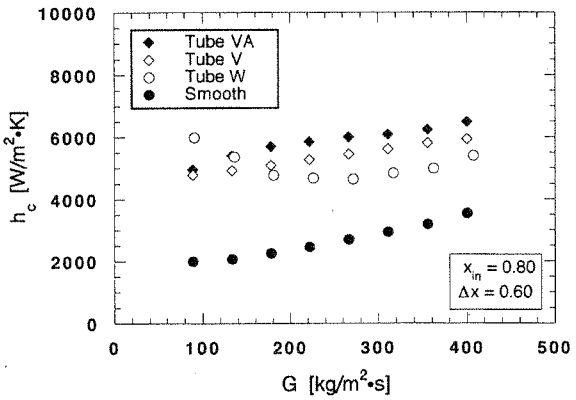

FIGURE 7 Condensation heat transfer coefficient versus mass flux for given inlet quality and quality change along test section.

function of mass flow rate for all tubes except the tube W. Data for this tube exhibit, indeed, a peculiar trend with a minimum for a mass flow rate of about 260 kg/s·m^2. A possible explanation can be probably found in terms of surface-tension forces that in conjunction with cross-section profile, which is characterised by a high number of fins with a large apex angle, could promote a condensate film thinning on fin tips like that in the Gregorig's effect (Gregorig [1954]). Thus, only for sufficiently large values of mass flux, shear stress forces predominate on surface forces and heat transfer coefficient becomes an increasing function of G. In Figure 8, condensation enhancement factors are plotted versus mass flux. Data for tubes VA and V show similar trends, i.e., weakly variable values at low G and a near constant decrement rate at intermediate and high G. Data for the tube W, instead, are characterised by a quite different trend which results roughly logarithmic. For values of G higher than 160 kg/s·m^2, the tube VA shows the most favourable enhancement factor. Finally, with the necessary caution due to the comparison between quantities referring to different conditions, heat transfer enhancement in evaporation seems to be higher -or much higher- than that in condensation at the lowest value of G but, for increasing values of mass flux, this deviation first vanishes and then reverses.

Figures 9, 11 and 12 present results for the evaporation pressure drop, obtained in the same conditions reported in Figures 3, 5 and 6, respectively. For all tubes, pressure drop is an increasing function of mass flow rate, vapor quality and quality change; however, its dependence on the vapor quality is weak and the influence of quality change seems to be negligible. Furthermore, microfin tubes display pressure drops higher than those of the smooth tube, even if the increment is 44% at the most. In Figure 10, the penalty factor, defined as the ratio of pressure

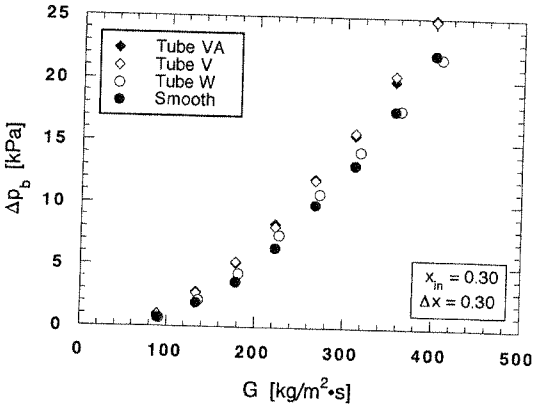

FIGURE 9 Evaporation pressure drop versus mass flux for given inlet quality and quality change along test section.

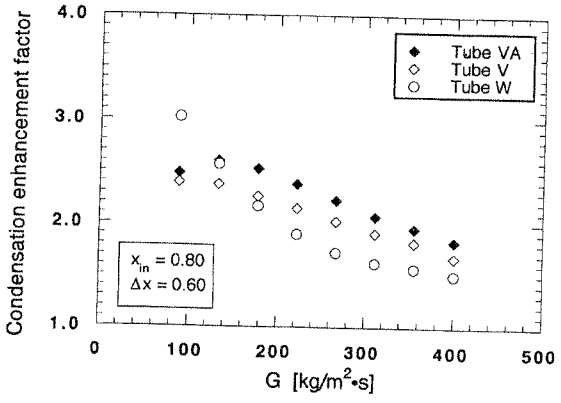

FIGURE 8 Condensation enhancement factor versus mass flux for given inlet quality and quality change.

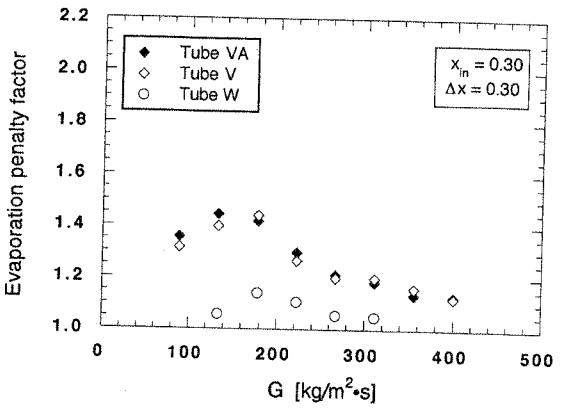

FIGURE 10 Evaporation penalty factor versus mass flux for given inlet quality and quality change along test section.

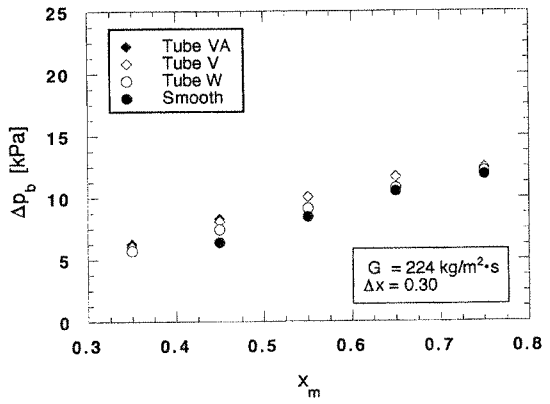

FIGURE 11 Evaporation pressure drop versus average vapor quality for given mass flux and quality change along test section.

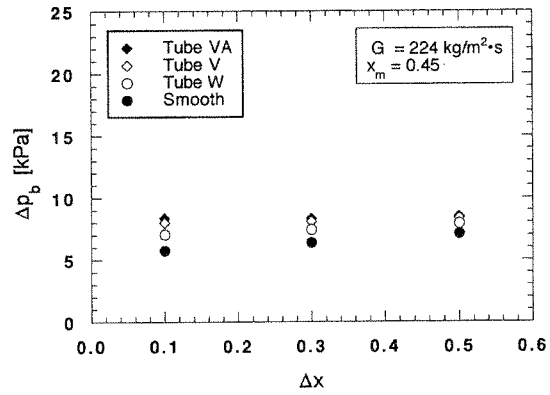

FIGURE 12 Evaporation pressure drop versus quality change for given mass flux and average vapor quality along test section.

drop of a microfin tube to that of the smooth tube, is plotted versus mass flux. Tubes V and VA essentially exhibit the same penalty factor, with values varying from 1.44 to 1.13 while G ranges between 160 and 400 kg/s·m^2. The tube W, instead, is characterised by a penalty factor about 20% lower, on the average, but with a trend similar to that of the other two microfin tubes. Finally, the penalty factor is not a strictly decreasing function of mass flow rate, as the enhancement factor, but it shows a maximum at low values of G.

Condensation pressure drops and the corresponding penalty factors, for $x_{in}=0.8$ and $x_{out}=0.2$, are plotted versus mass flux in Figures 13 and 14, respectively. Also in condensation, pressure drop is an increasing function of G with values, for microfin tubes, larger than those of the smooth tube. Penalty factors are up to 2.1, and therefore result quite higher than those in evaporation. The tube V shows the more favourable penalty factor, ranging between 1.5 and 1.05, whereas values for the tube VA result from 40% to 14% higher for G varying between 130 and 400 kg/s·m^2. Finally, the penalty factor for the tube W

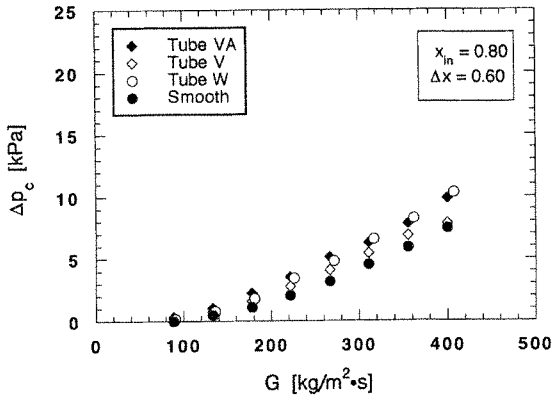

FIGURE 13 Condensation pressure drop versus mass flux for given inlet quality and quality change along test section.

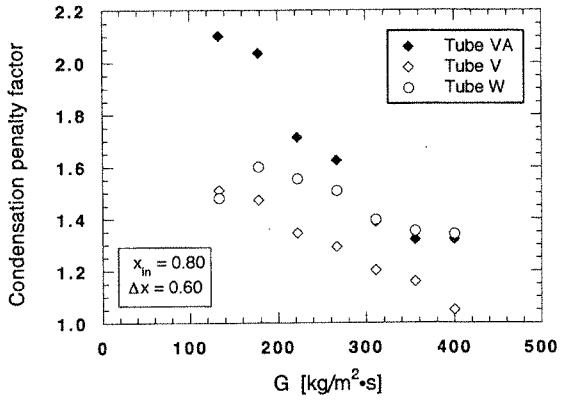

FIGURE 14 Condensation penalty factor versus mass flux for given inlet quality and quality change along test section.

displays values quite similar to those of the tube VA for G larger than 280 kg/s·m^2 while, for smaller G, it approaches data for the tube V.

Data for the smooth tube are compared with the predictions of several correlations from the literature. With local correlations, both the average heat transfer coefficient and the pressure drop are computed by numerical integration. Computation is based on the experimental values of heat rate with the assumption of uniform heat flux in each subsection, which is tantamount to suppose a linear variation of quality along subsection. Data for wall temperatures are not taken into account. In evaluating total pressure drop, the acceleration term is computed using the homogeneous model, if not otherwise stated by the particular correlation.

Figure 15 shows the comparison of experimental and predicted heat transfer coefficients plotted versus mass flux, for evaporation tests. Predictions are made through the correlations of Pierre [1964], that provides average heat transfer coefficients, Chawla [1967], Liu and Winterton [1991], and Kandlikar [1990] in the form recommended for refrigerants. As can be seen, the agreement with predictions of the Pierre and the Kandlikar correlations is particularly satisfying. Condensation heat transfer results are compared with the correlations of Shah [1979] and Cavallini and Zecchin [1972], and with correlations scheme of Butterworth [1983] and Paikert [1988]. As shown in Figure 16, the Shah correlation consistently underestimates experimental values of heat transfer coefficient. A much better agreement is exhibited by the correlation of Cavallini and Zecchin, particularly for the larger mass fluxes. This fact is not surprising if one considers that the correlation was proposed for the high velocity regime, that is in annular flow. In the calculation schemes proposed by Butterworth and by Paikert, allowance is made for the various condensation modes, namely, stratifying, annular and intermediate. It can be seen that the Paikert calculation scheme compares favourably with our experimental results, whereas the Butterworth procedure does not prove satisfactory.

Figures 17 and 18 show the comparison between experimental and predicted values of pressure drop in evaporation and condensation, respectively. The correlations of Chawla reported in VDI-Wärmeatlas [1974] and Grønnerud [1972] prove to be very good predictors both in evaporation and condensation. In evaporation, also the correlation proposed by Friedel [1979] was tested; as can be seen, experimental data are overpredicted at low mass flow rates, while they are underpredicted at high values of G. In condensation, a further comparison

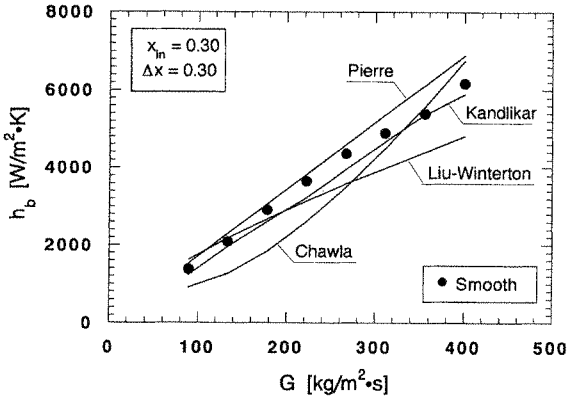

FIGURE 15 Comparison of experimental and predicted heat transfer coefficients plotted versus mass flux during flow-boiling inside the smooth tube.

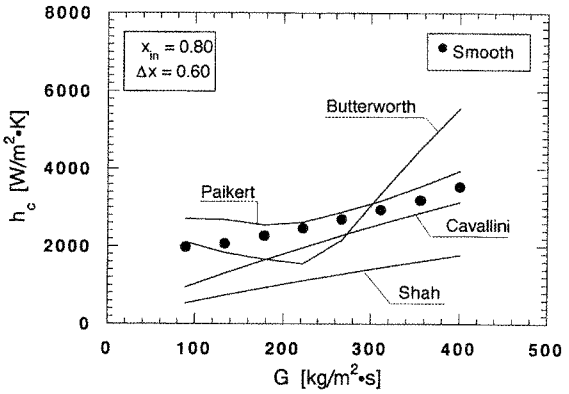

FIGURE 16 Comparison of experimental and predicted heat transfer coefficients plotted versus mass flux during condensation inside the smooth tube.

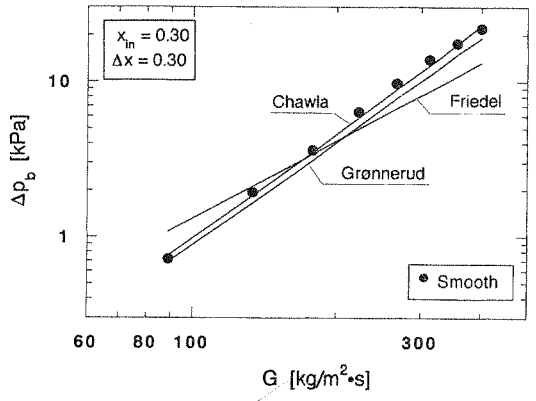

FIGURE 17 Comparison of experimental and predicted pressure drops plotted versus mass flux during flow-boiling inside the smooth tube.

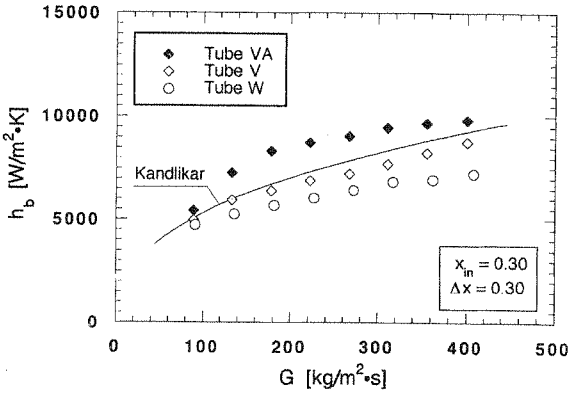

FIGURE 19 Comparison of experimental and predicted heat transfer coefficients plotted versus mass flux during flow-boiling inside microfin tubes.

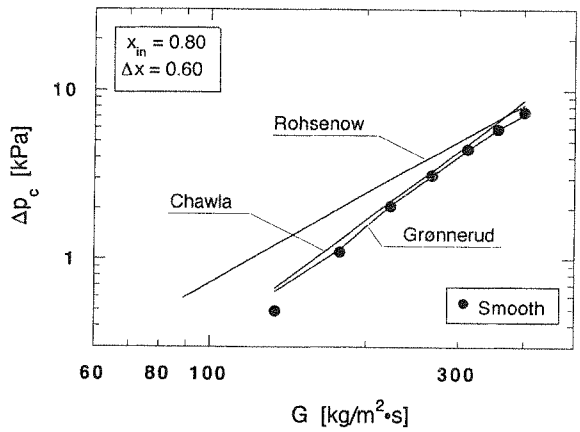

FIGURE 18 Comparison of experimental and predicted pressure drops plotted versus mass flux during condensation inside the smooth tube.

is made against Rohsenow correlation reported by Griffith and Rohsenow [1985], that was worked out for the annular flow. The evident convergence of such predictions to our experimental data, as mass flow rate is increased, points out the progressive achievement of the annular flow in the test section.

Finally, in Figure 19 the boiling coefficients for microfin tubes are plotted versus mass flux along with the predictions obtained by the correlation scheme recently proposed by Kandlikar and Raykoff [1996]. This correlation scheme contains three empirical constants, depending on the specific microfin geometry, which are the enhancement factors for nucleate and convective boiling terms, respectively, and the exponent of the Reynold's number in the single phase correlation. Thus, five different sets of these constants are given by Kandlikar for as many microfin tubes, included two much similar to our tube V. Since experimental coefficients for these two tubes were obtained within two distinct ranges of mass fluxes, i.e., 25–100 and 248–600 kg/s·m^2, we choose the set of constant values referring to the latter because the more close to our range. As can be seen, data for tube V correlate very well with Kandlikar estimates, while for the other microfin tubes only their trend is reflected by the curve.

It is noteworthy, however, to point out the enhancement factor for nucleate boiling term results 1.724 times that for convective boiling term, for the chosen constants set in the Kandlikar correlation. This circumstance implies a dependence of the boiling coefficient on quality, for fixed mass flux and quality change, different from the trend followed instead by our data, as can be seen in Figure 20. In fact, at low G, predictions show a decreasing trend with quality because the nucleate boiling term prevails over the convective one.

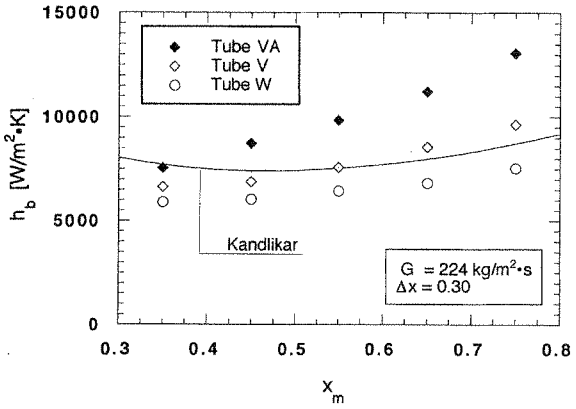

FIGURE 20 Comparison of experimental and predicted heat transfer coefficients plotted versus average vapor quality during flow-boiling inside microfin tubes.

Finally, regarding the dependence on the quality change, predictions display a slope, not shown, higher than that of our experimental data. However, in both cases, deviation between predicted and measured values of the boiling coefficient remains – excepting the point for $\Delta x = 0.5$ and $G = 224$ kg/s·m^2- always less than 17%, that is essentially within the mean error of the correlation scheme.

5. CONCLUSIONS

This work has presented experimental results for average heat transfer coefficient and pressure drop in saturated flow boiling and convective condensation inside three microfin tubes of different geometries (Metofin® W, V and VA) together with data for a smooth tube. All tubes have the same outer diameter. Whereas tubes V and W are more traditional, the tube VA is characterised by a new cross-section profile. In fact, such a tube has the peculiarity to alternate fins with two different heights, while it shares some geometric features, i.e., fin number and apex and helix angles, with other microfin tubes of new design as, for example, the Hitachi Thermofin-HEX™.

Data were collected varying the mass flow rate, the inlet thermodynamic quality, and the quality change between test section inlet and outlet. The tube VA shows the best thermal performance among the microfin tubes tested, especially in evaporation. For this case, the enhancement factor comes up to 4 and the heat transfer coefficient is 20% higher than that of the tube V on the average, while pressure drops remain essentially equal. This result, if confirmed in a wider range of values of the investigated parameters, could be due to the double height of fins, since other microfin tubes of new design seemingly display comparable enhancement factors but higher pressure drops.

Results for the smooth tube have been compared with predictions of several correlations. The good agreement of data with the values obtained by some of such correlations represent a satisfactory reliability check of the adopted experimental procedures. Finally, we have presented a comparison between the boiling coefficients for microfin tubes and the values predicted by Kandlikar and Raykoff correlation scheme. These predictions correlate well uniquely with data for the tube V, which has a geometry similar to one accounted by the scheme, while for the other microfin tubes only the trend with mass flow rate is retained. In fact, this correlation scheme cannot predict the geometry effect.

Eventually, we would further remark the need to understand how geometry affects the heat transfer mechanisms in order both to explain the better thermal performances of new microfin tubes and to make correlations predictive of the geometrical parameters. To this aim, experimental investigation is currently being carried out upon characterising flow patterns during evaporation and condensation, as well as single-phase heat transfer coefficients, inside microfin tubes.

Acknowledgments

The authors would like to thank Mr. Mario Corso and Mr. Augusto Trovati of the Dipartimento di Energetica of Politecnico di Milano for the invaluable assistance in the setting up the apparatus, and the manufacturer of the microfin tubes TREFIMETAUX (France), for supplying the tubes.

This work is supported by the Europa Metalli-LMI spa (Italy) and MURST.

NOMENCLATURE

A = area, m^2
D = diameter, m
G = mass flux, $kg/m^2 \cdot s$
h = heat transfer coefficient, $W/m^2 \cdot K$
m = mass flow rate, kg/s
p = pressure, Pa
Q = heat rate, W
q = heat flux, W/m^2
T = temperature, K(°C)
x = vapor quality
Δ = change in quantity

Subscripts

b = boiling
c = condensation
i = subsection index
in = inlet
m = mean
out = outlet
r = refrigerant
s = saturation condition
w = wall

References

Arosio, S., Muzzio, A. and Niro, A. (1995). Caratteristiche di scambio termico per R22 in ebollizione e in condensazione in un tubo microalettato (in Italian), Atti del *XIII Congresso Nazionale sulla Trasmissione del Calore UIT*, pp. 257–268.

Arosio, S., Muzzio, A. and Niro, A. (1996) Evaporation and condensation heat transfer and pressure drop of R22 inside microfin tubes, *2nd European Thermal Sciences and 14th UIT National Heat Transfer Conference 1996*, Eds. G. P. Celata, P. Di Marco, A. Mariani, **1**, pp. 227–234, ETS, Pisa I.

Bergles, A. E. (1994) Advanced Enhancement for Heat Exchangers, *Proc. The Japan-U.S. Seminar on Thermal Engineering for Global Enviromental Protection (A-5)*, pp. 1–14.

Butterworth, D. (1983) Film Condensation of Pure Vapor, in *Handbook of Heat Exchanger Design*, Hemisphere Publishing, Washington, DC, pp. 2.6.2/1–19.

Cavallini, A. and Zecchin, R. (1972) Scambio Termico nella Condensazione ad Alta Velocità di Fluidi Frigorigeni Organici entro Tubi: Dati Sperimentali e Correlazioni (in italian), in *La Termotecnica*, **XXVI**, n. 4, pp. 199–208.

Chawla, J. M. (1967) Wärmeübertragung und Druckabfall in waagerechten Rohren bei der Strömung von verdampenden Kältemitteln, in Kältetechnik-Klimatisirung, heft 8, pp. 246–252.

Darabi, J., Salehi, M., Saeedi, M. H. and Ohadi, M. M. (1995) Review of available correlations for prediction of flow boiling heat transfer in smooth and augmented tubes, in *ASHRAE Transactions*, **101**, Part 1, CH-95-12-2.

Friedel, L. (1979) Improved friction pressure drop correlations for horizontal and vertical two-phase pipe flow. European Two-Phase Flow Group Meeting, Ispra, Italy, Paper E2.

Gnielinski, V. (1983) Forced convection in ducts, in *Handbook of Heat Exchanger Design*, Hemisphere Publishing, Washington, DC, 2.5.1/1-11.

Gregorig, R. (1954) Hautkondensation an Feingewellten Oberflächen bei Berücksichtigung der Oberflächenspannungen, in *Z. Angew. Math. Phys.*, **5**, pp. 36–49.

Griffith, P. and Rohsenow, W. M. (1985) Condensation, in *Handbook of Heat Transfer Fundamentals*, McGraw Hill, New York, pp. 11/1-36.

Grønnerud, R. (1972) Investigation in Liquid Hold-up, Flow Resistance and Heat Transfer in Circulation Type Evaporators, Part IV: Two-Phase resistance in Boiling Refrigerants, in *Bull. de l'Inst. du Froid*, Annexe 1972-1.

Kandlikar, S. G. (1990) Flow Boiling Maps for Water, R22 and R134a in the Saturated Region, *Heat transfer 1990, Proc. 9th Int'l Heat Transfer Conference*, **2**, pp. 15–20.

Kandlikar, S. G. and Raykoff, T. (1996) Predicting flow boiling heat transfer for refrigerants in microfin tubes, in *2nd European Thermal-Sciences and 14th UIT National Heat transfer Conference*, Eds. G. P. Celata, P. Di Marco, A. Mariani, **1**, pp. 475–482, ETS, Pisa, I.

Kubanek, G. R. and Miletti, D. L. (1979) Evaporative Heat Transfer and Pressure Drop of Internally-Finned Tubes with Refrigerant 22, in *Journal of Heat Transfer*, **101**, pp. 447–452.

Liu, Z. and Winterton, R. H. S. (1991) A General Correlation for Saturated and Subcooled Flow Boiling in Tubes and Annuli Based on Nucleate Pool Boiling, in *Int. J. Heat Mass Transfer*, **34**, pp. 2759–2765.

Paikert, P. (1988) Wärmeübertragung bei Kondensation und Bemessung von Verflüssigern, in Handbuch der Kältetechnik, Springer-Verlag, Berlin, 6ter Band/Teil B.

Pierre, B. (1964) Flow Resistance with Boiling Refrigerants, in *ASHRAE J.* **6**, pp. 58–65.

Schlager, L. M., Pate, M. B. and Bergles, A. E. (1990) Evaporation and Condensation Heat Transfer and Pressure Drop in Horizontal, 12.7-mm Microfin Tubes with Refrigerant 22, in *Journal of Heat Transfer*, **112**, pp. 1041–1047.

Shah, M. M. (1979) A General Correlation for Heat Transfer during Film Condensation inside Pipes, in *Int. J. Heat Mass Transfer*, **22**, pp. 547–556.

Thome, J. R. (1990) *Enhanced Boiling Heat Transfer*, Hemisphere Publishing Co., Washington, DC, pp. 204–265.

Thome, J. R. (1994) Two-phase Heat Transfer to New Refrigerants, *Heat transfer 1994, Proc. 10th Int'l Heat Transfer Conference*, **1**, pp. 19–41.

VDI-Wärmeatlas (1974) Berechnungsblätter für den Wärmeübergang, in 2.Aufl. Düsseldorf: VDI-Verlag.

Webb, R. L. (1994) Advances in Modeling Enhanced Heat Transfer Surface, *Heat transfer 1994, Proc. 10th Int'l Heat Transfer Conference*, **1**, pp. 445–459.